

# Non-intrusive and semi-intrusive uncertainty quantification of a multiscale in-stent restenosis model

Dongwei Ye<sup>a,\*</sup>, Anna Nikishova<sup>a,\*</sup>, Lourens Veen<sup>b</sup>, Pavel Zun<sup>a,c,d</sup>,  
Alfons G. Hoekstra<sup>a</sup>

<sup>a</sup>*Computational Science Lab, Informatics Institute, Faculty of Science, University of Amsterdam, The Netherlands*

<sup>b</sup>*Netherlands eScience Center, Amsterdam, The Netherlands*

<sup>c</sup>*ITMO University, Saint Petersburg, Russia*

<sup>d</sup>*Erasmus University Medical Center, Rotterdam, The Netherlands*

---

## Abstract

Uncertainty estimations are presented of the response of a multiscale in-stent restenosis model, as obtained by both non-intrusive and semi-intrusive uncertainty quantification. The in-stent restenosis model is a fully coupled multiscale simulation of post-stenting tissue growth, in which the most costly submodel is the blood flow simulation. Surrogate modelling for non-intrusive uncertainty quantification takes the whole model as a black-box and maps directly from the three uncertain inputs to the quantity of interest, the neointimal area. The corresponding uncertain estimates matched the results from quasi-Monte Carlo simulations well. In the semi-intrusive uncertainty quantification, the most expensive submodel is replaced with a surrogate model. We developed a surrogate model for the blood flow simulation by using a convolutional neural network. The semi-intrusive method with the new surrogate model offered efficient estimates of uncertainty and sensitivity while keeping a relatively high accuracy. It outperformed the result obtained with earlier surrogate models. It also achieved the estimates comparable to the non-intrusive method with a similar efficiency. Presented results on uncertainty propagation with non-intrusive and

---

\*Corresponding authors

*Email addresses:* [d.ye@uva.nl](mailto:d.ye@uva.nl) (Dongwei Ye), [A.Nikishova@uva.nl](mailto:A.Nikishova@uva.nl) (Anna Nikishova), [L.Veen@esciencecenter.nl](mailto:L.Veen@esciencecenter.nl) (Lourens Veen), [Pavel.Zun@gmail.com](mailto:Pavel.Zun@gmail.com) (Pavel Zun), [A.G.Hoekstra@uva.nl](mailto:A.G.Hoekstra@uva.nl) (Alfons G. Hoekstra)

semi-intrusive metamodeling methods allow us to draw some conclusions on the advantages and limitations of these methods.

*Keywords:* Uncertainty Quantification, Sensitivity Analysis, Surrogate modelling, Semi-intrusive method, Gaussian process regression, Convolutional neural network, Multiscale simulation

---

## 1. Introduction

Numerical simulations of real-world phenomena contribute to a better understanding of these phenomena and to predicting the dynamics of the underlying systems. Many natural phenomena occur across scales in space and time [1, 2, 3, 4, 5, 6]. As a result, multiscale models and simulations are widely used [7, 8, 1, 9, 10]. These multiscale models couple mathematical models of relevant processes on different spatial or temporal scales together relying on suitable scale bridging methods [11]. However, multiscale simulations can suffer from substantial computational cost because of the high computational demands of, usually, the microscale simulations [10]. Uncertainty quantification (UQ) analysis [12] applied to multiscale simulations adds additional substantial computational burden since thousands of runs are required for good estimates of the uncertainties. Therefore simulations can become extremely time-consuming or impractical, even on current state-of-the-art supercomputing infrastructure.

To reduce the computational cost of multiscale UQ, we have recently proposed a set of semi-intrusive algorithms for multiscale UQ [13] and demonstrated their effectiveness for several multiscale UQ scenarios [13, 14]. Usually the output of a multiscale model is derived from a macroscale submodel, which in turn is implicitly determined by microscale dynamics to which it is coupled. One approach from [13] relies on performing a Monte Carlo UQ on the macroscale submodel while replacing the most costly microscale submodel by a surrogate model. The surrogate model is trained on existing data to learn the mapping between input and output and then makes a prediction for a new experiment based on the learned pattern. Replacing the expensive part of a model with

a relatively cheap surrogate can often significantly improve computational efficiency, but comes at the cost of reduced accuracy. In [14], a physics-based and an interpolation-based surrogate model were constructed to implement the semi-intrusive UQ for the in-stent restenosis multiscale model [15, 16, 17]. The results were compared to black-box Monte Carlo results to demonstrate the efficiency improvement. However, a comparison between the semi-intrusive algorithm and non-intrusive UQ with a surrogate model replacing the complete multiscale model were not explored in that study. In this work, we first improve the surrogate model of the micro-scale model (the blood flow simulation) from [14] by using a convolutional neural network (CNN), due to its capability of pattern recognition and feature extraction [18, 19]. Additionally, a surrogate model for non-intrusive UQ is designed to directly map the input parameters to the quantity of interest. The UQ estimations with both these methods are then carried out and compared in terms of the UQ estimation and computational efficiency.

The paper is arranged as follows. The two-dimensional multiscale model of in-stent restenosis is shortly introduced in Section 2. The new surrogate model for the blood flow simulation and the surrogate model for the in-stent restenosis model are described in Section 2.2. The approach to estimate and analyse the uncertainty of the response of the in-stent restenosis model is explained in Section 3. The results of surrogate modelling, uncertainty quantification and sensitivity analysis are presented in Section 4. Sections 5 and 6 compare and discuss the UQ performance and summarise the obtained results.

## 2. Model

### 2.1. In-stent Restenosis

An arterial stenosis is the abnormal narrowing of an artery, usually due to accumulation of fatty material in the walls and intimal thickening (atherosclerosis). In ischemic heart disease, a stenosis in a coronary artery limits blood flow to the heart muscle, which can result in reduced heart function, shortness of breath, chest pains or a heart attack. Coronary stenosis can be treated using

balloon angioplasty, in which a balloon is inserted into the artery via a catheter and inflated, which compresses the fatty plaque against the arterial wall. During this procedure, a wire-mesh stent is deployed to keep the artery from recoiling back to the narrowed state. This procedure damages the vessel wall, and in particular the endothelium, the innermost lining of the artery. This triggers a healing response involving (amongst other processes) growth and proliferation of smooth muscle cells (SMCs) on the inside of the artery. In some cases, an excessive growth response occurs, leading to a significant renewed narrowing of the artery inside of the stent. This is known as an in-stent restenosis (ISR), and is considered an adverse treatment outcome [20, 21, 22].

The ISR2D model is a two-dimensional simulation of the post-stenting healing response of an artery [16, 17], which is used here to test the proposed semi-intrusive multiscale UQ algorithm. Note that a more realistic, but also computationally much more expensive three dimensional version of the model is available [23, 24]. The ISR2D model used in this paper consists of three sub-models: the IC submodel, which simulates initial conditions in the form of the state of the artery immediately after stenting, the SMC submodel, which is an agent-based simulation of smooth muscle cell growth and endothelium recovery, and the blood flow submodel, which uses the Lattice Boltzmann method (LBM) to simulate blood flow through the artery. The structure of ISR2D is shown in Figure 1.

Sufficiently high wall shear stress (WSS) at the arterial wall triggers any present endothelium to produce nitric oxide, which in turn inhibits the growth of the SMCs if it crosses a threshold value. Blood flow thus affects SMC growth, but in turn is also affected by it, as the proliferating SMCs change the geometry of the artery. Note that due to random placement of daughter cells when the growing SMCs divide, variability in the length of the cell cycle, and a random spatial pattern of endothelium recovery, the SMC model is stochastic. The main output of the model is the cross-sectional area of the neointima (the new tissue formed due to SMC proliferation) as a function of time after stenting. A clinically recognised in-stent restenosis occurs if more than 50% of the original

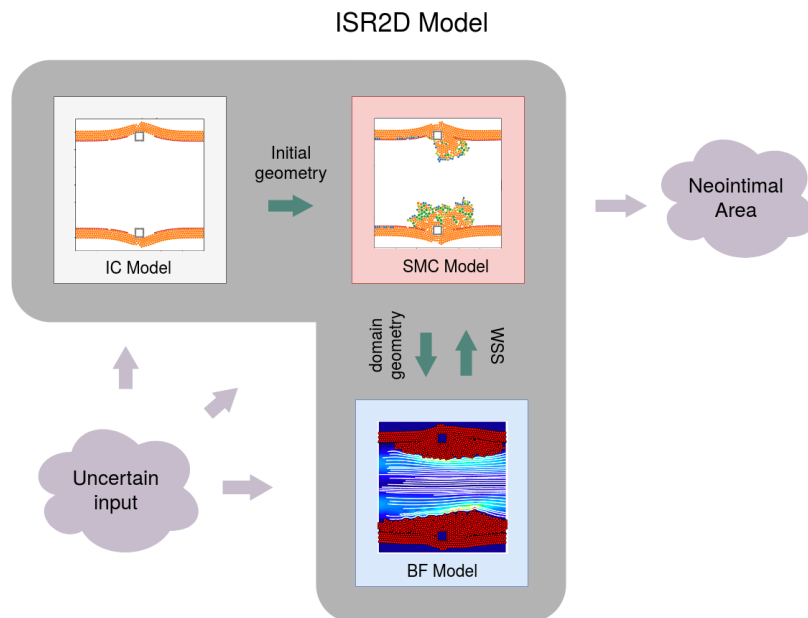


Figure 1: Diagram of the ISR2D model: the initial conditions (IC) submodel provides the initial geometry to the smooth muscle cells (SMC) single scale model where the geometry is further updated. SMC model calls the blood flow (BF) simulation, which provides the wall shear stress (WSS) for the updated geometry. The cycle continues until the final time step is reached, when the SMC model yields the final output of the cross-sectional area.

cross-sectional area of the artery is covered by the neointima [25].

The SMC growth occurs over a period of weeks, while blood flow adapts much more rapidly to the changing geometry. ISR2D is therefore a multiscale model exhibiting time-scale separation. For every time step of the SMC model (one time step simulates one hour resulting in 1440 steps per 60 days of the total simulation time), the BF simulation is run to convergence for the current geometry, and the resulting WSS values are sent back to the SMC model, which uses those in the model of nitric oxide production by endothelial cells.

Figure 2 shows an input (domain map) and corresponding output (shear stress field) of the BF submodel. The domain map represents the geometry of the artery in the form of a binary grid, with 1 (shown in black) representing a solid grid cell, and 0 (shown in white) representing a fluid grid cell. The output

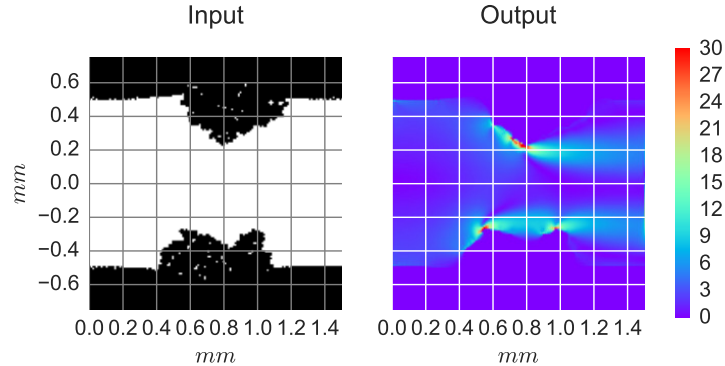


Figure 2: Input and output of blood flow simulation. Left plot:  $150 \times 150$  binary geometry map as the input for blood flow simulation. The black part is the vessel wall and the white part is the lumen (the fluid domain). Right plot: Simulated shear stress in the domain (in  $Pa$ ).

of the BF simulation is a corresponding grid of shear stress values, which are set to 0 for solid domain cells, and set to the shear stress values computed by LBM for fluid domain cells. The shear stresses at the fluid-solid boundary layer are taken as the wall shear stresses and passed to the SMC model.

The blood flow simulation is the computationally most expensive component of the ISR2D model. It takes around 80% of the computational time, and the potential gain in performance obtained by replacing it with a surrogate model in the semi-intrusive UQ scenario is therefore highest. Nikishova et al. performed a semi-intrusive UQ analysis for the same model, comparing surrogates based on nearest-neighbour interpolation and on simplified physics to a non-intrusive black box Monte Carlo approach [14]. The UQ estimates with physics surrogate has improved the computational efficiency but the means of the cross-sectional area of the neointima resulting from the surrogate models were substantially lower than the black-box Monte Carlo result. On the other hand, the UQ estimates with nearest-neighbour interpolation is better but the corresponding speedup was relatively poor. In this paper, an accurate surrogate model using convolutional neural network is proposed and demonstrated to result in accurate estimates of the uncertainties, while at the same time leading to the desired

reduction in computational cost for the multiscale UQ.

## 2.2. Surrogate Model for Blood Flow Simulation

As mentioned in the previous section, the blood flow simulation in the ISR2D model is computationally expensive. To reduce the computational cost of the model, a surrogate model to compute the required wall shear stresses is used to replace the original blood flow model. Convolutional neural networks have been applied to fetch the features from irregular geometries in fluid dynamics prediction [18, 26, 19]. In ISR2D application, the aim is to learn the latent nonlinear function between vessel wall geometry, blood flow velocity and wall shear stress.

The mapping between input and output of the BF simulation can be considered as a function  $f$ , which takes the geometry matrix  $\zeta$  and the inlet blood velocity  $v_{\text{in}}$  as input and produces a  $2 \times k$ -dimensional vector of WSS magnitudes,  $\tau_{\text{wss}}$  as the output:

$$\tau_{\text{wss}} = f(\zeta, v_{\text{in}}), \quad (2.1)$$

where  $k = 150$  is the grid size along x axis,  $\zeta = (\zeta_{ij}) \in \mathbb{R}^{k \times k}$ . The geometry matrix  $\zeta$  was used for CFD simulation. The surrogate model  $\hat{f}$  replaces the original blood flow model  $f(\zeta, v_{\text{in}})$  and offers an approximate prediction of wall shear stress in a reduced amount of time.

The CNN model follows the network structure proposed by [18] and was optimized to fit our application. The model consists of three parts: shape encoding, nonlinear mapping and stress decoding, as shown in Figure 3. The shape encoding layers extract the features of the geometry to the shape code. A fully connected (FC) layer then maps the shape code together with the blood flow velocity to the stress code. The stress decoding part is responsible for a mapping from the stress code to wall shear stress. In this surrogate model, the geometry input was transformed from a binary map to a  $2 \times k$  array which indicates the locations of upper and lower fluid-solid boundaries. The convolution layers then take the information from both boundaries into account and predict the shear stress on these boundaries. There are three convolution layers, a fully

connected layer and three deconvolution layers deployed between the input layer and output layer. Each of them is followed by a rectifier linear unit (ReLU) as the activation function. Besides, the output of each convolution layer is concatenated to the corresponding deconvolution layer to help with the decoding process.

The training data for the surrogate model comes from the runs of the ISR2D model [27]. One run of ISR2D calls the LBM solver 1440 times (once per hour of simulated time). This means that with only a few runs of the simulation, a considerable amount of flow data for training is already available. We trained the surrogate model with the data from four runs of ISR2D simulation, hence 5760 blood vessel geometries and wall shear stress distributions were used for training. The training optimization was based on the mean squared error loss function:

$$\mathcal{L}(\tau_{wss}) = \frac{1}{n} \sum_{i=1}^n \|\tau_{wss}^{(i)} - \hat{\tau}_{wss}^{(i)}\|^2 \quad (2.2)$$

where  $n$  denotes the number of samples of the training set. The *Adam* optimizer

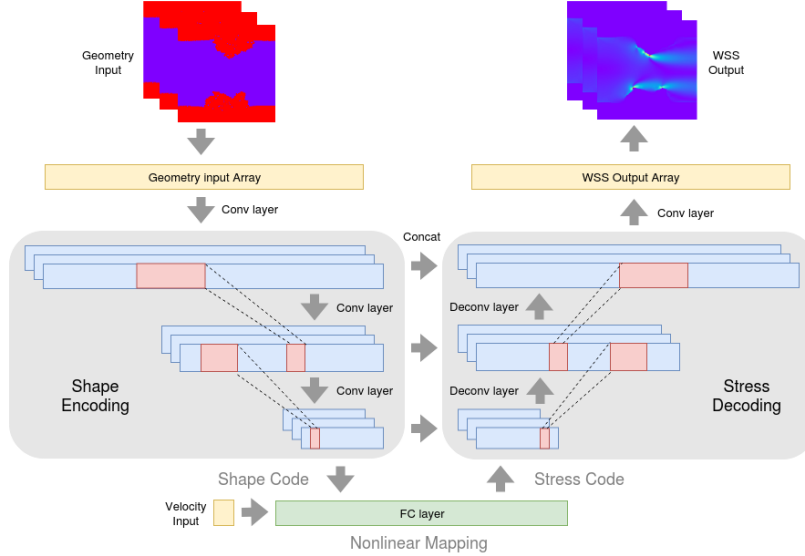


Figure 3: Diagram of the CNN model



was used to optimize the hyper-parameters in the model. A validation against a test dataset was done during the training process to prevent the model from overfitting. The epoch was set to 80 as the loss does not decrease significantly after that. The surrogate model was implemented in Keras [28].

### 2.3. Surrogate Model for ISR2D

This surrogate model is constructed to replace the whole ISR2D multiscale model for uncertainty quantification and sensitivity analysis. Let the multi-scale model function be defined by  $g(\xi)$  with  $\xi$  denoting a  $n$ -dimensional vector consisting of the stochastic variables and uncertain inputs of the model. The response of the model is:

$$y = g(\xi) \tag{2.3}$$

As mentioned before, the ISR2D model is a stochastic model and thus includes both aleatory uncertainty and epistemic uncertainty. In the surrogate model for non-intrusive UQ, we assume that the aleatory uncertainty can be separated from the function  $g$ , hence the expression for the surrogate model can be written as:

$$\hat{y} = h(\xi_{\sim\xi^*}) + \epsilon(\xi^*) \tag{2.4}$$

where  $\hat{y}$  denotes the response of the surrogate model,  $\xi^*$  is the aleatory uncertainty and  $\xi_{\sim\xi^*}$  is the parameter vector without stochastic variable. Assuming that the aleatory uncertainty  $\epsilon$  follows a normal distribution  $N(0, \sigma^{*2})$ , such a stochastic model can be easily quantified by Gaussian process regression (GPR). Note that ISR2D is a time-evolving model, and that we are not only interested in the response at the final timestep, but also in the process. To avoid an extra dimension of input, more precisely, a time  $t$  that will significantly increase the computational cost of training and prediction [29], a local surrogate model for each time step is constructed. Therefore the expression can be rewritten as:

$$\hat{y}_t = h_t(\xi_{\sim\xi^*}) + \epsilon_t(\xi^*), \quad t = 1, 2, \dots, T, \tag{2.5}$$

GPR is based on the assumption of the joint Gaussian distribution between training data and prediction mean:

$$\begin{pmatrix} y_t^{\text{train}} \\ h_t^{\text{pred}} \end{pmatrix} \sim N \left( 0, \begin{bmatrix} K_t + \sigma_t^* I & K_t^* \\ (K_t^*)^T & K_t^{**} + \sigma_t^* I \end{bmatrix} \right), \quad t = 1, 2, \dots, T \quad (2.6)$$

where covariance matrices  $K_t$ ,  $K_t^{**}$  and  $K_t^*$  denote the correlation within training data, within test data, and between these two respectively at each time step. Applying Bayesian inference, the posterior probability distribution of  $h_t^{\text{pred}}$  given training set

$(\xi_{\sim \xi^*}^{\text{train}}, y_t^{\text{train}})$  follows a Gaussian process:

$$P(h_t^{\text{pred}} | (\xi_{\sim \xi^*}^{\text{train}}, y_t^{\text{train}}), \xi_{\sim \xi^*}^{\text{pred}}) = \mathcal{GP}(\bar{h}_t^{\text{pred}}, \text{Var}(h_t^{\text{pred}})), \quad (2.7)$$

where

$$\bar{h}_t^{\text{pred}} = K_t^* (K_t + \sigma_t^* I)^{-1} y_t^{\text{train}}$$

and

$$\text{Var}(h_t^{\text{pred}}) = K_t^{**} - K_t^* (K_t + \sigma_t^* I)^{-1} (K_t^*)^T.$$

The mean value offers the prediction and the variance represents the uncertainty of this prediction. The radial basis function kernel and white noise kernel were chosen for the computation of covariance matrices. In each local GPR model, there are three hyperparameters associated to the kernels, length scale  $l_t$ , signal variance  $\sigma_t^f$  and noise variance (stochasticity)  $\sigma_t^*$ . These hyperparameters are trained by optimizing log marginal likelihood function:

$$\begin{aligned} \log p(y_t^{\text{train}} | \xi_{\sim \xi^*}) &= -\frac{1}{2} (y_t^{\text{train}})^\top (K_t + \sigma_t^{*2} I)^{-1} y_t^{\text{train}} \\ &\quad - \frac{1}{2} \log |K_t + \sigma_t^{*2} I| - \frac{n}{2} \log 2\pi. \end{aligned} \quad (2.8)$$

The training data comes from the qMC result from [27] and the size of the training data was chosen to match the speedup of semi-intrusive UQ. As the semi-intrusive method gains a speedup of around 7, the speedup of the non-intrusive method is also designed to be around 7 for comparison. Therefore, 150 ISR2D simulations are used for training. The Gaussian process surrogate model used in non-intrusive UQ was built using GPy [30].

### 3. Uncertainty quantification and sensitivity analysis

Uncertainty Quantification is the analysis of the precision of a computational model [31], including uncertainty in the model response (*forward problem*), and its input (*inverse problem*). Here, the forward propagation of uncertainty and the precision of the ISR2D model output are studied.

The semi-intrusive metamodeling method involves replacing a computationally expensive single-scale submodel with a surrogate, which produces an approximation to the original single scale model result in a reduced time. The input uncertainty is propagated via the surrogate model in the same way as for the non-intrusive method, by running an ensemble with parameter values sampled from a distribution. Using the obtained samples of the model response, uncertainty in the model is estimated, analysing the probability density function, mean and variance, as well as estimating the Sobol sensitivity indices [32, 33]. The mean and variance of the model responses at time step  $t$  are then estimated by:

$$\begin{aligned}\mathbb{E}(\hat{y}_t(\xi)) &\approx \frac{1}{N} \sum_{j=1}^N \hat{y}_t(\xi_j), \\ \text{Var}(\hat{y}_t(\xi)) &\approx \frac{1}{N} \sum_{j=1}^N \hat{y}_t(\xi_j)^2 - \left( \frac{1}{N} \sum_{j=1}^N \hat{y}_t(\xi_j) \right)^2,\end{aligned}\tag{3.1}$$

where  $N$  is the number of samples. The Sobol sensitivity index for the  $i$ -th parameter is defined by

$$S_{\xi_i}^{total} = \frac{\text{Var}_{\xi_i}^{total}(\hat{y}_t(\xi))}{\text{Var}(\hat{y}_t(\xi))},\tag{3.2}$$

where the partial variance in the numerator is approximated by [34, 35]

$$\text{Var}_{\xi}^{total}(\hat{y}_t(\xi_i)) \approx \frac{1}{2N} \sum_{j=1}^N \left( \hat{y}_t(\xi^j) - \hat{y}_t(\xi_{\sim i}^j, \xi_i^{j+N}) \right)^2,\tag{3.3}$$

where  $\xi_{\sim i}$  is a vector of all elements of  $\xi$  except the  $i$ -th element, and  $g(\xi_{\sim i}^j, \xi_i^{j+N})$  denotes the model response with the same values of all inputs as for  $g(\xi^j)$  except the  $i$ -th input  $\xi_i$ .

It is important to note that since ISR2D is a stochastic model, the estimates of the partial variance for the uncertain inputs include the aleatory uncertainty as well. The aleatory uncertainty was estimated on its own using Eq. 3.3, taking advantage of the fact that two model runs with the same input values give  $g(\xi^j)$  and  $g(\xi_{\sim\xi^*}^j, \xi_{\xi^*}^{j+N})$ .

## 4. Results

First, the quality of the blood flow surrogate model is evaluated. Then, the results of UQ and sensitivity analysis based on non-intrusive and semi-intrusive methods are compared to a previously obtained reference solution reported in [27].

### 4.1. Blood flow surrogate model

Before applying the blood flow surrogate model to semi-intrusive UQ analysis, the quality of the surrogate model was evaluated. We used normalized mean absolute error (NMAE) on the test dataset to evaluate the quality of the surrogate model:

$$\text{NMAE} = \frac{\frac{1}{2k} \|\tau_{wss} - \hat{\tau}_{wss}\|}{\max\{|\tau_{wss}|\}} \times 100\%, \quad (4.1)$$

where  $\|\cdot\|$  denotes  $L_1$  norm and  $\max\{|\tau_{wss}|\}$  is the peak stress in the LBM. Figure 4 visualizes the wall shear stress prediction of the CNN surrogate model and the LBM solver on a test dataset (CFD simulation results in one ISR2D simulation). The averaged NMAE of the surrogate model on the whole test dataset is around 3.33%. The results show that the CNN surrogate model approximates the wall shear stress well in most cases. The prediction gets slightly worse close to the outlet of blood flow. The relatively poor prediction may be caused by extrapolation, since the growth is stochastic, and the lumen geometry may end up with a previously unseen irregular shape which is not covered by the training dataset.

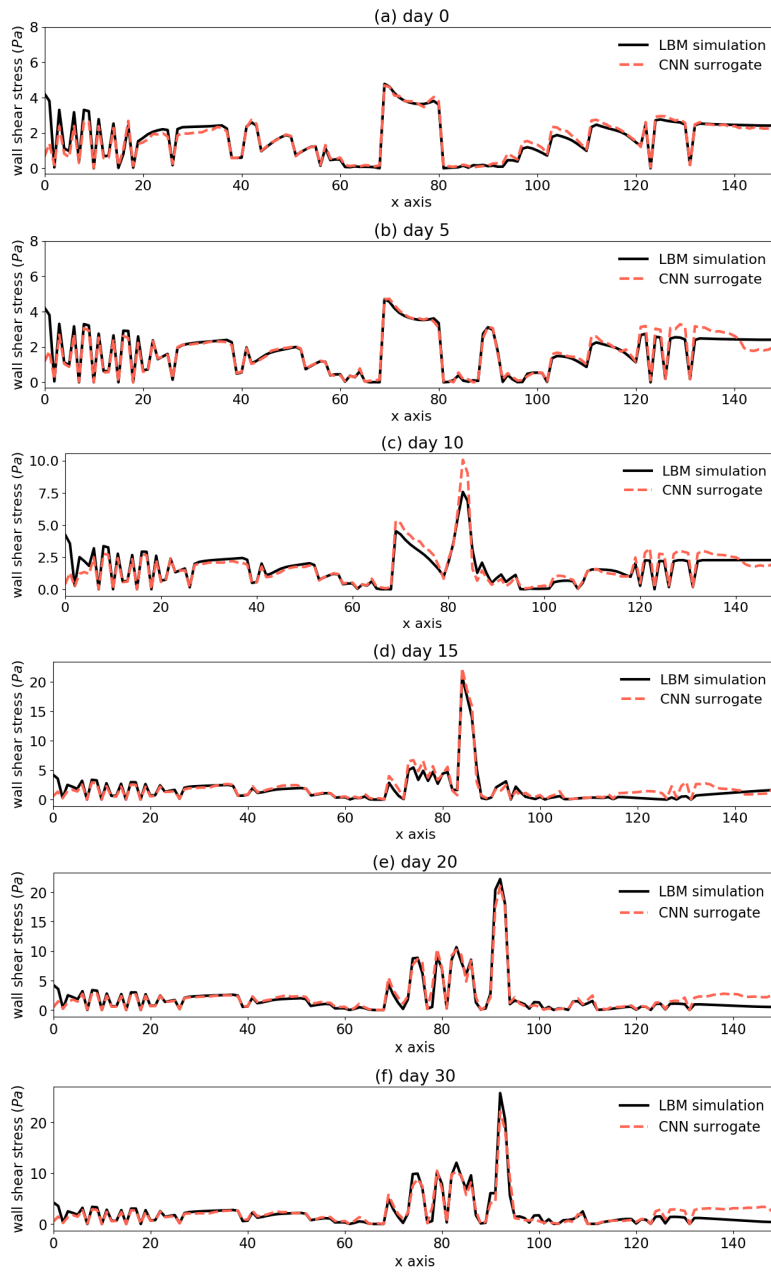


Figure 4: (a) - (f) Predictions of wall shear stress distribution along the upper boundary by LBM and CNN surrogate models at 0, 5, 10, 15, 20, 30 days. The corresponding NMAEs are 4.14%, 4.15%, 5.2%, 2.67%, 2.49% and 2.88%

Uncertain Parameter	Range (min)	Range (max)	Unit
inlet blood flow velocity	0.432	0.528	m/s
maximum deployment depth	0.09	0.13	mm
endothelium regeneration time	15	23	days

Table 1: List of UQ parameters of ISR2D and their min and max values.

#### 4.2. Uncertainty quantification and sensitivity analysis

Uncertainty in the ISR2D model response is due to the model stochasticity and uncertainty in three model parameters. The ranges of the uncertain parameters are shown in Table 4.2. These three uncertain inputs are assumed to be uniformly distributed within the given ranges. The model output of interest was the neointimal area as a function of time after stenting and its uncertainty was estimated using non-intrusive method (NI) and semi-intrusive (SI) method with surrogates of the blood flow micro model. We compared the uncertainty quantification result and sensitivity analysis result for similar values of UQ speedup. We also show the quasi-Monte Carlo (qMC) result from [27] as the reference solution. The total number of model runs in both qMC and SI experiments was 1024.

Figure 5 shows the estimates of the mean and standard deviation with the qMC, the SI and NI methods. The mean is approximated especially well for the first 10 simulated days. After this point, slightly less average growth is observed in both SI and NI estimates than in the qMC results. The NI estimates slightly outperformed the SI estimates. The shape of the mean value of the neointimal area is well approximated by both SI method and NI method. The results of the standard deviation from the SI and NI methods also show approximately similar value to the qMC estimator.

The comparison of the probability density functions (pdf) obtained with three UQ methods at 5, 10, 15, 20 and 60 days after stenting are shown in Figure 6. A good fit of the pdfs is obtained at the early time points. For day 5 and day 10, the two sample Kolmogorov-Smirnov (K-S) test for qMC and SI

pdfs produces statistics of 0.04 and 0.07 respectively, while the statistics between qMC and NI stays at 0.05. At later time points, the K-S statistic is always smaller for the results of NI estimates than with SI estimates, which means a better fit. These plots also indicate the ratio of restenosis cases defined by 50% occlusion of the original lumen area [25] (shown as the vertical line). Non-zero values of this ratio are only observed at day 20 and 60. As expected, prediction of a smaller growth in SI resulted in a relatively smaller predicted binary restenosis rate. The NI’s prediction is closer to the qMC result. At the final simulation time point, NI predicted 10.3% restenosis occurrence while SI predicted 7.7% occurrence. A summary of uncertainty estimation at the final time step by different methods is presented in Table 2. The NI estimations have the smallest error in the estimation of the mean and the restenosis ratio. The SI with CNN results have a smaller error than some other methods for each estimator. All the SI and NI results show a statistically significant underestimation of the mean value (two-value t-test,  $p < 0.01$ ).

Figure 7 illustrates the overall and the partial variances and Sobol sensitivity indices as quantified using SI, NI and qMC. These quantities were overestimated to a certain degree by the NI method but all the estimates are still within the confidence interval of the qMC results and the order of the partial variances is

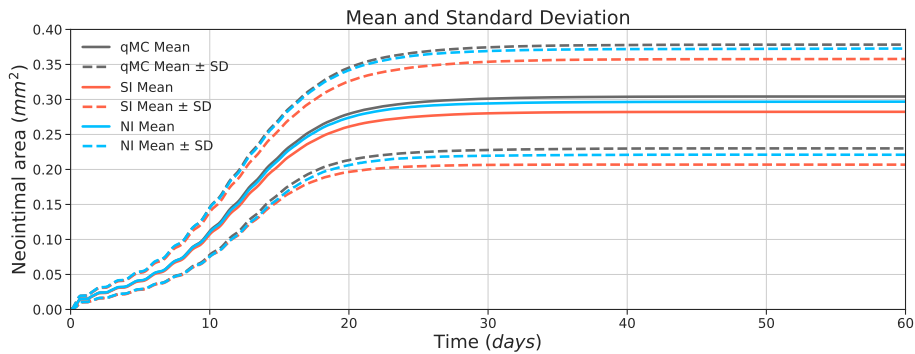


Figure 5: Mean and standard deviation of the ISR2D model output on the neointimal area with quasi-Monte Carlo (qMC) and with the semi-intrusive (SI) method and non-intrusive (NI) method.

UQ Method	Micro Model	Mean Estimation		Standard Deviation		Restenosis Ratio	
		$\times 10^{-1}$ (mm <sup>2</sup> )		$\times 10^{-2}$ (mm <sup>2</sup> )		(%)	
		Value	Error	Value	Error	Value	Error
qMC	LBM <sup>1</sup>	3.04	0	7.41	0	12.2	0
SI	DD I <sup>2</sup>	2.88	0.16	7.43	0.02	8.3	3.9
SI	DD II <sup>2</sup>	2.79	0.25	7.51	0.10	6.3	5.9
SI	Phys <sup>2</sup>	2.26	0.78	7.98	0.57	1.1	11.1
SI	CNN	2.82	0.22	7.54	0.13	7.7	4.5
NI	/	2.97	0.05	7.58	0.17	10.3	1.9

<sup>1</sup> From [27].

<sup>2</sup> From [14].

Table 2: Comparison of the estimates of means and standard deviation of neointimal growth and restenosis ratio with qMC, SI and NI methods. The indicated error is the absolute difference from the reference qMC value. The four surrogate models for SIUQ are data-driven model I (DD I), data-driven model II (DD II), physics surrogate model (Phys) and convolutional neural network model (CNN). See [14] for details on the Phys, and DD I and DD II surrogates.

preserved. Since both the overall and the partial variances are overestimated, the error is significantly smaller in the estimation of the sensitivity indices, and the indices obtained by NI method with GP are close enough to the one estimated by qMC. The variances estimated by the SI method are also close to the qMC result and all within its confidence interval. As a result, the total sensitivity indices are also well approximated with this type of method.

### 4.3. Speedup

The main purpose of applying SI and NI methods is to speed up the simulation and reduce the computational cost while getting good enough estimates of the uncertainties. The speedup of the UQ analysis of these advanced methods was computed as follows:

$$\mathcal{S} = \frac{N\mathcal{T}_{\text{ISR}}}{N\mathcal{T}_{\text{ISR}^*} + \mathcal{T}_{\text{train}} + \mathcal{T}_{\text{sample}}} \quad (4.2)$$

where  $N$  is the number of runs of ISR2D simulation in the UQ analysis.  $\mathcal{T}_{\text{ISR}}$  is the execution time of an ISR2D simulation with LBM solver.  $\mathcal{T}_{\text{ISR}^*}$  is the execution time of either an ISR2D simulation with a blood flow surrogate model



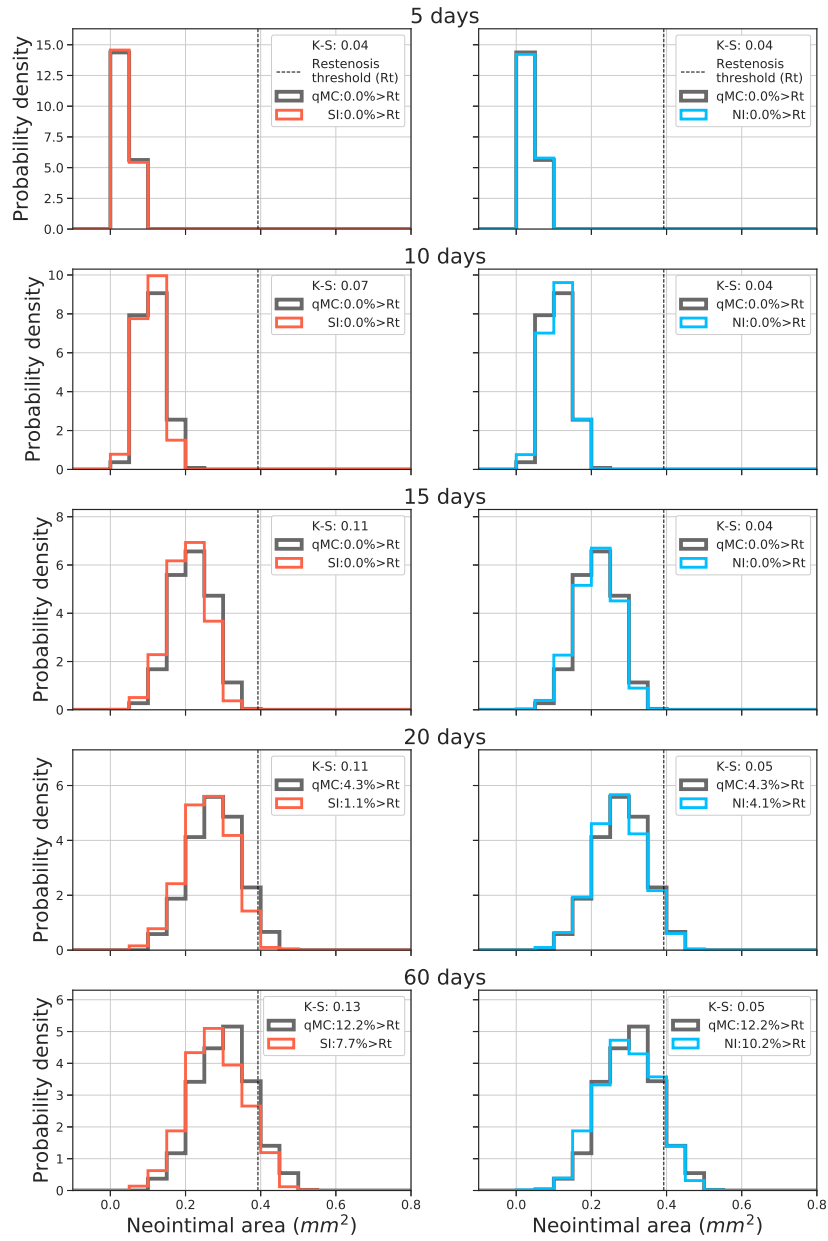


Figure 6: Probability density function of the neointimal area at different simulation times obtained with the quasi-Monte Carlo (QMC), the semi-intrusive method (SI) and non-intrusive method (NI).

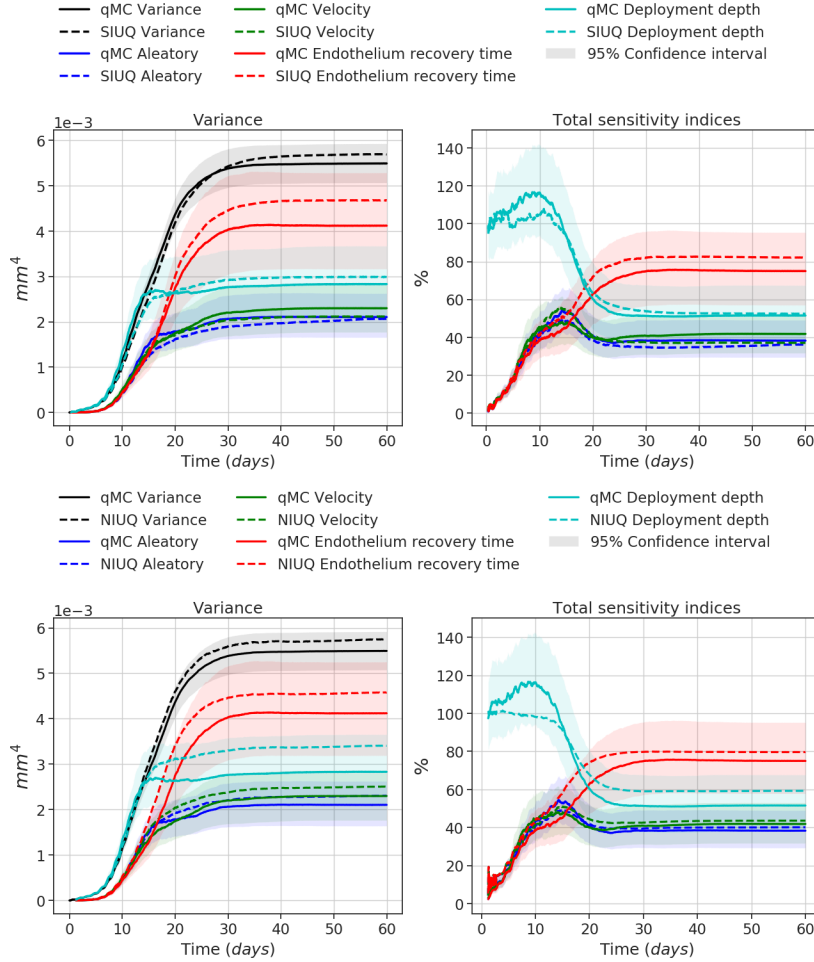


Figure 7: Partial and total variances (left column) and total Sobol sensitivity indices (right column) with qMC in solid lines and the SI (top row) and NI (bottom row) in dashed lines. Each of the quantities for the uncertain inputs includes the aleatory uncertainty. The area around the qMC results is the 95% confidence interval obtained by a bootstrap test [36].

or the execution time of the surrogate model of non-intrusive method.  $\mathcal{T}_{\text{train}}$  denotes the training time for the surrogate model.  $\mathcal{T}_{\text{sample}}$  denotes the time to generate the training data for the surrogate model. In Table 3, the execution times and resulting speedups of the SI and NI methods relative to the qMC method are evaluated, including previously reported SI results from [14] for

UQ Method	Micro Model	$\mathcal{T}_{\text{ISR}}$ (min)	$\mathcal{T}_{\text{ISR}^*}$ (min)	$\mathcal{T}_{\text{micro}}$ (min)	$\mathcal{T}_{\text{train}}$ (min)	$\mathcal{T}_{\text{sample}}$ (min)	N	Speedup of UQ
qMC	LBM <sup>1</sup>	89.4	/	74.9	/	/	1024	1
SI	DD I <sup>2</sup>	/	50.9	37.8	/	894	1024	1.72
SI	DD II <sup>2</sup>	/	14.6	2.05	/	447	1024	5.94
SI	Phys <sup>2</sup>	/	11.9	0.08	/	/	1024	7.51
SI	CNN	/	12.8	0.26	9.9	357.6	1024	6.79
NI	/	/	0.17	/	4.3	$1.1 \times 10^4$	1024	6.82

<sup>1</sup> From [27].

<sup>2</sup> From [14].

Table 3: Comparison of the computational time and corresponding speedup of different approaches. The time value indicates the mean computational time obtained over  $N = 1024$  samples.  $\mathcal{T}_{\text{micro}}$  is the execution time of micro model (LBM/surrogate models) in one ISR2D simulation. The all computations were performed on the Distributed ASCI Supercomputer DAS5 [37] with Intel Haswell E5-2630-v3 CPU.

comparison. Because of the light surrogate model, the SI approach with CNN was approximately seven times faster than black-box qMC, an improvement of more than a factor three over the nearest-neighbour interpolation based surrogate model. The simplified physics model was even faster, but was also the least accurate one, while the SI with CNN based surrogate model provided the best uncertainty quantification and sensitivity estimates among the four surrogates (see [14] for details on the Phys, and DD I and DD II surrogates).

## 5. Discussion

The CNN surrogate model performed well regarding the wall shear stress prediction for the micro model. It takes advantage of convolution layers to fetch latent features in the geometry input and then uses the FC layer and deconvolution layers to map the features to the wall shear stress prediction. Although the CNN surrogate model was able to predict the wall shear stress quite accurately, a small error still exists. This error introduced by the surrogate model then propagated through the iteration and led to the error in the UQ estimation and restenosis prediction as shown in Figure 5 and table 2. The accuracy of the SIUQ estimation depends not only on the quality of the surrogate

model but also on the structure of the multiscale simulation. However, the UQ result from the SI method suggests that the error is small enough to produce uncertainty and sensitivity estimates close to the ones obtained by qMC. Of course, the UQ result can be further improved by a better CNN surrogate model, e.g by training with a larger dataset or constructing a deeper CNN structure. But such improvement in the surrogate model does not necessarily guarantee a significant improvement in the UQ estimation. A trial experiment has been performed on ISR2D with a better CNN surrogate model (NMAE  $\approx 1\%$ ), but the improvement of the corresponding UQ estimates was minuscule.

The UQ estimates with CNN surrogate model outperformed the result of most previous surrogate models except DD I. The result with DD I is still slightly better which may be due to the large training dataset it used [13]. However the obtained speedup of DD I is much lower than the CNN model, since the CNN model learned the latent pattern of the data, while DD I simply looked for similar cases among all the training data. Because of this, the prediction cost of CNN is significantly lower. The maximum expected speedup of SIUQ with a surrogate model is limited by the computational cost of the macro model in the multiscale simulation. It can be calculated by  $\mathcal{T}_{\text{ISR}}/\mathcal{T}_{\text{macro}}$  which is around six for ISR2D. However the speedup of the SIUQ with CNN surrogate model (Table 3) is even higher than the maximum expected value. This is because the computational cost of the SMC (macro) model varies. It mainly depends on the number of agents in the model. As the ISR2D with a surrogate model underestimates the neointimal growth which means fewer agents in the SMC model, the corresponding computational time is reduced from 14 minutes to 12 minutes and even less. Thus, the computational burden of the SIUQ method comes mostly from the cost of the simulation multiplied by the number of samples and it is not affected visibly by the cost of obtaining the surrogate model. Although the deployment of the surrogate model reduces the computational cost, the maximum speedup is still limited by the computational cost of the other parts of the multiscale simulation. The main computational cost of NIUQ stems from the generation of training data. Consequently, there is

no upper limit for the speedup of NIUQ as long as the surrogate model can be efficiently and effectively trained with a small amount of data, e.g by applying active learning [38, 39]. Of course, the exact amount of data required to train a surrogate model for NIUQ depends not only on the dimensionality of the input but also on the desired accuracy. Therefore, selecting which method to apply for achieving an efficient UQ analysis has to take into consideration the multiscale model itself and the requirement of the UQ analysis.

By comparing the SI and NI results at the same computational efficiency, one can see that uncertainty and sensitivity analysis of SI were as good as the NI. SI has the additional advantage of granularity, since only part of the model is replaced by the surrogate. This means that the parameters of the submodels not replaced by the surrogate can be varied and studied without changing the surrogate, as long as the replaced micro model is not affected. For example, in case of the ISR2D model, different parameters and rule sets for cell behaviour can be used with the existing surrogate model for flow. On the other hand, using a NI model for a different biological ruleset would require essentially building a new NI surrogate, which would incur a significant computational cost.

In general, both SI and NI approaches performed well. The SI approach is more suitable for cyclic multiscale simulations as it retains the framework of the simulation and can obtain the training data for the surrogate model at a relatively low cost. Another semi-intrusive UQ strategy is to run the simulations for UQ and build the surrogate model on the fly. Such a dynamic system should be capable of constructing and updating the surrogate during the simulation process, for instance, as done by Leiter et al. [40]. In the UQ scenario, the surrogate model can also be validated dynamically [13]. We aim to apply these techniques to the three-dimensional versions of the ISR model in future work.

## 6. Conclusion

In order to implement uncertainty quantification and sensitivity analysis efficiently for the ISR2D model, a new surrogate model based on a convolutional

neural network was developed and applied in semi-intrusive UQ estimation. The UQ estimate with the new surrogate model was compared with the result of previous work and a non-intrusive UQ estimates based on Gaussian process regression. The result shows that SI with the convolutional neural network surrogate model outperformed the previous result. The result is also comparable to non-intrusive estimates. Both SI and NI are valid methods to perform UQ in an efficient way for the ISR2D model.

## 7. Funding

This work was supported by the Netherlands eScience Center under the e-MUSC (Enhancing Multiscale Computing with Sensitivity Analysis and Uncertainty Quantification) project. This project has received funding from the European Union Horizon 2020 research and innovation programme under grant agreements #800925 (VECMA project) and #777119 (InSilc project). PZ has received funding from The Russian Foundation for Basic Research under agreement #18-015-00504. This work was sponsored by NWO Exacte Wetenschappen (Physical Sciences) for the use of supercomputer facilities, with financial support from the Nederlandse Organisatie voor Wetenschappelijk Onderzoek (Netherlands Organization for Science Research, NWO).

## References

### References

- [1] A. Hoekstra, B. Chopard, P. Coveney, Multiscale modelling and simulation: a position paper, *Phil. Trans. R. Soc. A* 372 (2021) (2014) 20130377. doi:10.1098/rsta.2013.0377.
- [2] D. Groen, S. J. Zasada, P. V. Coveney, Survey of multiscale and multiphysics applications and communities, *Computing in Science & Engineering* 16 (2) (2014) 34–43. doi:10.1109/MCSE.2013.47.

- [3] A. Mizeranschi, D. Groen, J. Borgdorff, A. G. Hoekstra, B. Chopard, W. Dubitzky, *Anatomy and Physiology of Multiscale Modeling and Simulation in Systems Medicine*, Springer New York, New York, NY, 2016, pp. 375–404. doi:10.1007/978-1-4939-3283-2\_17.
- [4] S. Alowayyed, D. Groen, P. V. Coveney, A. G. Hoekstra, Multiscale computing in the exascale era, *Journal of Computational Science* 22 (2017) 15 – 25. doi:10.1016/j.jocs.2017.07.004.  
URL <http://www.sciencedirect.com/science/article/pii/S1877750316302988>
- [5] B. Chopard, J.-L. Falcone, P. Kunzli, L. Veen, A. Hoekstra, Multiscale modeling: recent progress and open questions, *Multiscale and Multidisciplinary Modeling, Experiments and Design* 1 (1) (2018) 57–68. doi:10.1007/s41939-017-0006-4.  
URL <https://doi.org/10.1007/s41939-017-0006-4>
- [6] A. G. Hoekstra, B. Chopard, D. Coster, S. P. Zwart, P. V. Coveney, Multiscale computing for science and engineering in the era of exascale performance, *Philosophical Transactions of the Royal Society A: Mathematical, Physical and Engineering Sciences* 377 (2142) (2019) 20180144. doi:10.1098/rsta.2018.0144.  
URL <https://royalsocietypublishing.org/doi/abs/10.1098/rsta.2018.0144>
- [7] M. Praprotnik, L. D. Site, K. Kremer, Multiscale simulation of soft matter: From scale bridging to adaptive resolution, *Annual Review of Physical Chemistry* 59 (1) (2008) 545–571, PMID: 18062769. doi:10.1146/annurev.physchem.59.032607.093707.
- [8] P. M. Slood, A. G. Hoekstra, Multi-scale modelling in computational biomedicine, *Briefings in bioinformatics* 11 (1) (2010) 142–152. doi:10.1093/bib/bbp038.

- [9] S. Karabasov, D. Nerukh, A. Hoekstra, B. Chopard, P. V. Coveney, Multiscale modelling: approaches and challenges, *Phil. Trans R. Soc. A* 372 (2021) (2014) 20130390. doi:10.1098/rsta.2013.0390.  
URL <https://royalsocietypublishing.org/doi/abs/10.1098/rsta.2013.0390>
- [10] S. Alowayyed, D. Groen, P. V. Coveney, A. G. Hoekstra, Multiscale computing in the exascale era, *Journal of Computational Science* doi:10.1016/j.jocs.2017.07.004.
- [11] B. Chopard, J. Borgdorff, A. G. Hoekstra, A framework for multi-scale modelling, *Phil. Trans R. Soc. A* 372 (2021) (2014) 20130378. doi:10.1098/rsta.2013.0378.
- [12] R. C. Smith, *Uncertainty quantification: theory, implementation, and applications*, Vol. 12, Siam, 2013.
- [13] A. Nikishova, A. G. Hoekstra, Semi-intrusive uncertainty propagation for multiscale models, *Journal of Computational Science* 35 (2019) 80 – 90. doi:10.1016/j.jocs.2019.06.007.  
URL <http://www.sciencedirect.com/science/article/pii/S1877750318313711>
- [14] A. Nikishova, L. Veen, P. Zun, A. G. Hoekstra, Semi-intrusive multiscale metamodelling uncertainty quantification with application to a model of in-stent restenosis, *Phil. Trans R. Soc. A* 377 (2142) (2019) 20180154. doi:10.1098/rsta.2018.0154.  
URL <https://royalsocietypublishing.org/doi/abs/10.1098/rsta.2018.0154>
- [15] D. J. Evans, P. V. Lawford, J. Gunn, D. Walker, D. Hose, R. Smallwood, B. Chopard, M. Krafczyk, J. Bernsdorf, A. Hoekstra, The application of multiscale modelling to the process of development and prevention of stenosis in a stented coronary artery, *Phil. Trans R. Soc. A* 366 (1879) (2008) 3343–3360.



- [16] H. Tahir, A. G. Hoekstra, E. Lorenz, P. V. Lawford, D. R. Hose, J. Gunn, D. J. W. Evans, Multi-scale simulations of the dynamics of in-stent restenosis: impact of stent deployment and design, *Interface Focus* 1 (3) (2011) 365–373. doi:10.1098/rsfs.2010.0024.
- [17] H. Tahir, C. Bona-Casas, A. G. Hoekstra, Modelling the effect of a functional endothelium on the development of in-stent restenosis, *PLoS One* 8 (6) (2013) e66138. doi:10.1371/journal.pone.0066138.
- [18] X. Guo, W. Li, F. Iorio, Convolutional neural networks for steady flow approximation, in: *Proceedings of the 22Nd ACM SIGKDD International Conference on Knowledge Discovery and Data Mining, KDD '16*, ACM, New York, NY, USA, 2016, pp. 481–490. doi:10.1145/2939672.2939738. URL <http://doi.acm.org/10.1145/2939672.2939738>
- [19] L. Liang, M. Liu, C. Martin, W. Sun, A deep learning approach to estimate stress distribution: a fast and accurate surrogate of finite-element analysis, *Journal of The Royal Society Interface* 15 (138) (2018) 20170844. doi:10.1098/rsif.2017.0844. URL <https://royalsocietypublishing.org/doi/abs/10.1098/rsif.2017.0844>
- [20] J. W. Jukema, J. J. W. Verschuren, T. A. N. Ahmed, P. H. A. Quax, Restenosis after PCI. Part 1: pathophysiology and risk factors., *Nature reviews. Cardiology* 9 (1) (2012) 53–62. doi:10.1038/nrcardio.2011.132. URL <http://www.ncbi.nlm.nih.gov/pubmed/21912414>
- [21] J. W. Jukema, T. A. N. Ahmed, J. J. W. Verschuren, P. H. A. Quax, Restenosis after PCI. Part 2: prevention and therapy., *Nature reviews. Cardiology* 9 (2) (2012) 79–90. doi:10.1038/nrcardio.2011.148. URL <http://www.ncbi.nlm.nih.gov/pubmed/21989052>
- [22] J. Iqbal, P. W. Serruys, D. P. Taggart, Optimal revascularization for complex coronary artery disease., *Nature reviews. Cardiology* 10 (11) (2013)

635–47. doi:10.1038/nrcardio.2013.138.

URL <http://www.ncbi.nlm.nih.gov/pubmed/24042217>

- [23] P. S. Zun, T. Anikina, A. Svitenkov, A. G. Hoekstra, A comparison of fully-coupled 3d in-stent restenosis simulations to in-vivo data, *Frontiers in Physiology* 8 (2017) 284. doi:10.3389/fphys.2017.00284.

URL <https://www.frontiersin.org/article/10.3389/fphys.2017.00284>

- [24] P. S. Zun, A. J. Narracott, C. Chiastra, J. Gunn, A. G. Hoekstra, Location-Specific Comparison Between a 3D In-Stent Restenosis Model and Micro-CT and Histology Data from Porcine In Vivo Experiments, *Cardiovascular Engineering and Technology* 10 (4) (2019) 568–582. doi:10.1007/s13239-019-00431-4.

URL <http://link.springer.com/10.1007/s13239-019-00431-4>

- [25] P. W. Serruys, J. A. Ormiston, Y. Onuma, E. Regar, N. Gonzalo, H. M. Garcia-Garcia, K. Nieman, N. Bruining, C. Dorange, K. Miquel-Hbert, et al., A bioabsorbable everolimus-eluting coronary stent system (absorb): 2-year outcomes and results from multiple imaging methods, *The Lancet* 373 (9667) (2009) 897910. doi:10.1016/s0140-6736(09)60325-1.

- [26] J. Tompson, K. Schlachter, P. Sprechmann, K. Perlin, Accelerating eulerian fluid simulation with convolutional networks, in: *Proceedings of the 34th International Conference on Machine Learning - Volume 70, ICML'17*, JMLR.org, 2017, pp. 3424–3433.

URL <http://dl.acm.org/citation.cfm?id=3305890.3306035>

- [27] A. Nikishova, L. Veen, P. Zun, A. G. Hoekstra, Uncertainty quantification of a multiscale model for in-stent restenosis, *Cardiovascular Engineering and Technology* 9 (4) (2018) 761–774. doi:10.1007/s13239-018-00372-4.

- [28] F. Chollet, et al., Keras, <https://keras.io> (2015).

- [29] C. E. Rasmussen, C. K. I. Williams, Gaussian Processes for Machine Learning (Adaptive Computation and Machine Learning), The MIT Press, 2005.
- [30] GPy, GPy: A gaussian process framework in python, <http://github.com/SheffieldML/GPy> (since 2012).
- [31] W. L. Oberkampf, S. M. DeLand, B. M. Rutherford, K. V. Diegert, K. F. Alvin, Error and uncertainty in modeling and simulation, *Reliability Engineering & System Safety* 75 (3) (2002) 333 – 357. doi:10.1016/S0951-8320(01)00120-X.  
URL <http://www.sciencedirect.com/science/article/pii/S095183200100120X>
- [32] I. M. Sobol, On sensitivity estimation for nonlinear mathematical models, *Matematicheskoe Modelirovanie* 2 (1) (1990) 112–118.
- [33] S. Kucherenko, M. Rodriguez-Fernandez, C. Pantelides, N. Shah, Monte Carlo evaluation of derivative-based global sensitivity measures, *Reliability Engineering & System Safety* 94 (7) (2009) 1135 – 1148, Special Issue on Sensitivity Analysis. doi:10.1016/j.ress.2008.05.006.
- [34] T. Homma, A. Saltelli, Importance measures in global sensitivity analysis of nonlinear models, *Reliability Engineering & System Safety* 52 (1) (1996) 1 – 17. doi:10.1016/0951-8320(96)00002-6.
- [35] A. Saltelli, P. Annoni, I. Azzini, F. Campolongo, M. Ratto, S. Tarantola, Variance based sensitivity analysis of model output. Design and estimator for the total sensitivity index, *Computer Physics Communications* 181 (2) (2010) 259–270. doi:10.1016/j.cpc.2009.09.018.
- [36] G. E. B. Archer, A. Saltelli, I. M. Sobol, Sensitivity measures, ANOVA-like Techniques and the use of bootstrap, *Journal of Statistical Computation and Simulation* 58 (2) (1997) 99–120. doi:10.1080/00949659708811825.
- [37] H. Bal, D. Epema, C. de Laat, R. van Nieuwpoort, J. Romein, F. Seinstra, C. Snoek, H. Wijshoff, A medium-scale distributed system for computer

science research: Infrastructure for the long term, *Computer* 49 (5) (2016) 54–63. doi:10.1109/MC.2016.127.

[38] T. Collet, O. Pietquin, Optimism in active learning with gaussian processes, in: S. Arik, T. Huang, W. K. Lai, Q. Liu (Eds.), *Neural Information Processing*, Springer International Publishing, Cham, 2015, pp. 152–160.

[39] D. R. Jones, M. Schonlau, W. J. Welch, Efficient global optimization of expensive black-box functions, *Journal of Global optimization* 13 (4) (1998) 455–492.

[40] K. W. Leiter, B. C. Barnes, R. Becker, J. Knap, Accelerated scale-bridging through adaptive surrogate model evaluation, *Journal of Computational Science* 27 (2018) 91 – 106. doi:10.1016/j.jocs.2018.04.010.

URL <http://www.sciencedirect.com/science/article/pii/S1877750317313807>